ADVANCED ENGINEERING MATERIALS

DOI: 10.1002/adem.201200203

Processing and Characterization of In Situ $(TiC–TiB_2)_p$/AZ91D Magnesium Matrix Composites**

By *Mohammed Shamekh, Martin Pugh* and *Mamoun Medraj**

In this paper, a practical and cost-effective processing route, in situ reactive infiltration technique, was utilized to fabricate magnesium matrix composites reinforced with a network of TiC–TiB_2 particulates. These ceramic reinforcement phases were synthesized in situ from Ti and B_4C powders without any addition of a third metal powder such as Al. The molten Mg alloy infiltrates the preform of ($Ti_p + B_4C_p$) by capillary forces. The microstructure of the composites was investigated using scanning electron microscope (SEM)/energy dispersive X-ray spectroscopy (EDS). The compression behavior of the composites processed at different conditions was investigated. Also, the flexural strength behavior was assessed through the four-point-bending test at room temperature. Microstructural characterization of the (TiB_2–TiC)/AZ91D composite processed at 900 °C for 1.5 h shows a relatively uniform distribution of TiB_2 and TiC particulates in the matrix material resulting in the highest compressive strength and Young's modulus. Compared with those of the unreinforced AZ91D Mg alloy, the elastic modulus, flexural and compressive strengths of the composite are greatly improved. In contrast, the ductility is lower than that of the unreinforced AZ91D Mg alloy. However, this lower ductility was improved by the addition of MgH_2 powder in the preform. Secondary scanning electron microscopy was used to investigate the fracture surfaces after the flexural strength test. The composites show signs of mixed fracture; cleavage regions and some dimpling. In addition, microcracks observed in the matrix show that the failure might have initiated in the matrix rather than from the reinforcing particulates.

In recent years, the demand for magnesium is increasing especially in automotive and aerospace applications due to their light weight. Weight reduction is considered the best cost-effective option for significant reduction in fuel consumption and in CO_2 emission.[1] However, the use of Mg alloys in automotive and aerospace applications has been limited because of their rapid loss of strength with increasing temperature, low elastic modulus, low wear resistance at elevated temperatures, poor creep resistance, high coefficient of thermal expansion, and poor corrosion resistance.[2,3] AZ91 alloy is one of the most widely used Mg-based engineering materials, which exhibits excellent mechanical properties over pure Mg especially when it is heat-treated.[3]

Mg matrix composites reinforced with suitable ceramic particles such as TiC and TiB_2 compensate for some of the limitations of Mg alloys and improve their properties.[4] Moreover, since composites are flexible in constituent selection, their properties can be tailored more than what can be achieved by alloying elements.[2,5] Besides, compared to Mg alloys, Mg matrix composites can be considered as an excellent alternative because of their higher specific stiffness, higher specific strength, high wear resistance, and good elevated temperature creep properties.[6] Hence, the demand for Mg matrix composites for the automotive and aerospace components such as automotive pulleys, cog-tooth sprockets, oil-pump covers, cylinder liners, and aircraft engine casings is increasing.[7]

Mg matrix composites reinforced with in situ TiC and TiB_2 particles has been fabricated by different techniques such as self-propagating high temperature synthesis (SHS) and remelting and dilution.[8,9] These techniques depend on adding a metal powder such as Al to Ti–B_4C preform in fabricating TiB_2–TiC/Mg matrix composites because aluminum acts as a reaction intermediary to facilitate the reaction between Ti and B_4C. However, high Al content leads to the formation of the interdentritic grain boundary

[*] *Dr. M. Shamekh, Prof. M. Pugh, Prof. M. Medraj*
Department of Mechanical Engineering,
Concordia University, 1455 de Maisonneuve Blvd. W., Montréal, Québec, Canada, H3G 1M8
E-mail: mmedraj@encs.concordia.ca

[**] *The authors thank Egyptian ministry of defense for giving the first author the opportunity to accomplish this work at Concordia University and for financial support from NSERC.*

phase $Mg_{17}Al_{12}$ leading to limited ductility of the matrix.[10] The BCC structure of $Mg_{17}Al_{12}$ is not coherent with the HCP structure of Mg leading to a weak Mg/$Mg_{17}Al_{12}$ interface. Also, at elevated temperatures, grain boundary sliding can take place due to the poor thermal stability and the discontinuous precipitation of the γ-phase inside the Mg matrix.[11] As a result, Mg alloys containing Al suffer from poor strength at elevated temperatures and low creep resistance.[12]

Compression properties of Mg matrix composites are very important for the structural parts used in the automotive industry because the automotive parts are often loaded under compression at room or elevated temperatures.[11] Flexural strength is the maximum tensile stress of a beam in bending and is a suitable alternate for the tensile test for not only brittle ceramic materials but also for ceramics reinforced composites.

Accordingly, the primary aim of this study is to synthesize Mg matrix composites reinforced with TiC and TiB_2 particulates using an in situ reactive infiltration technique. It is the first time such (TiC–TiB_2)/Mg matrix composites are fabricated starting from Ti and B_4C materials without adding Al using this practical and low cost technique. Microstructure, physical, and mechanical properties of the composites were studied. The compression behavior of the composites at different processing parameters was investigated. Also, their flexural strength behavior was assessed at room temperature. Finally, the effect of adding MgH_2 powder to the Ti–B_4C preform to control the volume percentage of the reinforcing phases and to tailor the mechanical properties of the composites was investigated.

1. Results and Discussion

1.1. Fabrication of the (TiC–TiB_2)/AZ91D Matrix Composites

The primary objective of this work is to find the optimal processing parameters for producing sound Mg matrix composites. To reach this goal, composite samples were fabricated using AZ91D as a matrix metal at different processing parameters such as temperature, holding time, and the green compact relative density (RD). This study was conducted by changing one factor at a time, while the particle sizes of Ti and B_4C and conditions of ball milling of the mixture (time and speed) were kept constant.

The results reveal the significant effect of the processing parameters on the fabrication of the composite. It was observed that the composites fabricated using a 3Ti–B_4C green compact of 70% RD at 900 °C for 1.5 h gives a relatively uniform distribution of the reinforcing phases, TiC_x and TiB_2, as a network in the matrix. Very small amount of residual Ti, boron carbide, and intermediate phases such as TiB, Ti_3B_4, and MgB_2 were observed as shown in the microstructure and elemental mapping in Figure 1 and the X-ray diffraction (XRD) patterns in Figure 2. No significant oxidation of Mg and formation of traces of the ternary compound (Ti_2AlC) were observed when the composites were fabricated at these processing parameters.

The elemental mapping reveals the overlap of the titanium, carbon, and boron images proving the existence of the network of TiC and TiB_2 in the Mg matrix. However, it is difficult to distinguish between the TiC and Ti borides phases because of the small difference in their mean atomic numbers making the discernment very difficult by SEM.

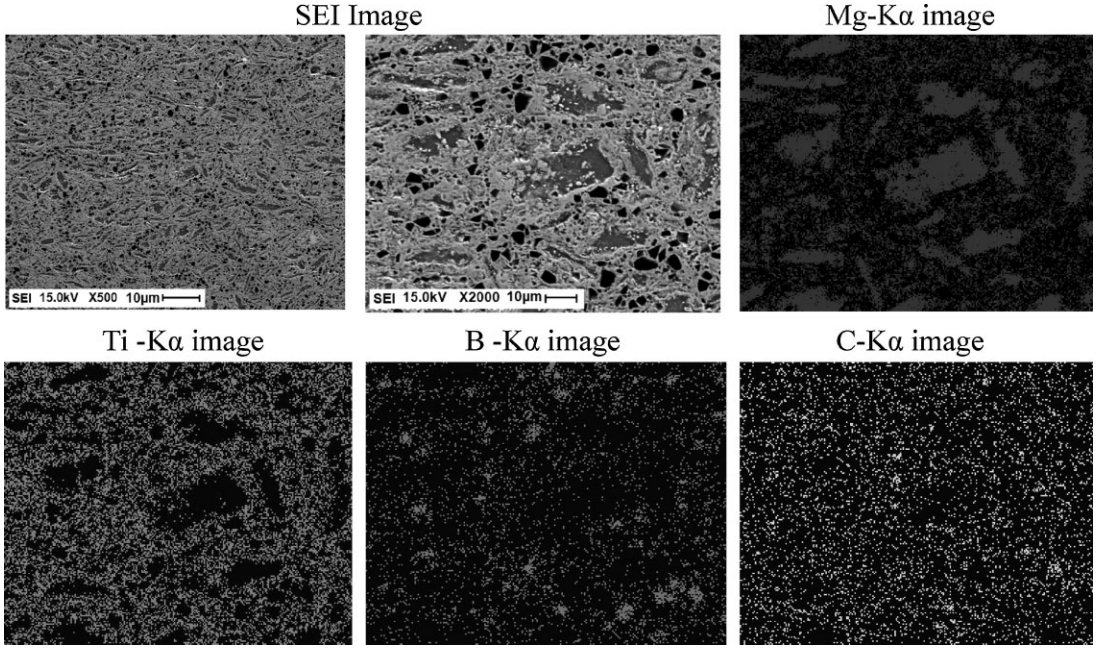

Fig. 1. SEM microstructure and EDS elemental mapping of the TiC_x–TiB_2/AZ91D composites synthesized using a 3Ti–B_4C preform with 70% RD at 900 °C for 1.5 h.

ADVANCED ENGINEERING MATERIALS **2013**,
DOI: 10.1002/adem.201200203

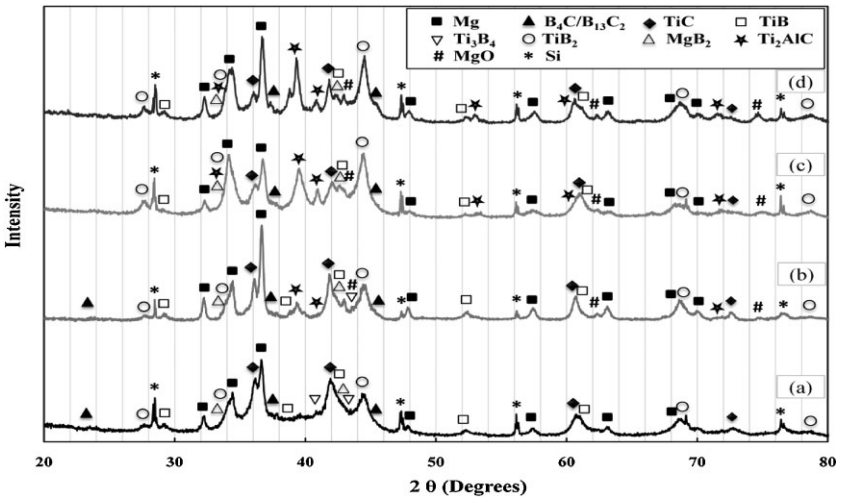

Fig. 2. XRD pattern of the AZ91D alloy MMCs fabricated using a 3Ti–B_4C preform with 70% RD at 900 °C for different holding times: (a) 1 h, (b) 1.5 h, (c) 3 h, and (d) 6 h.

On the other hand, AZ91D matrix composites have also been fabricated at these processing parameters but using an MgH_2–(3Ti–B_4C) preform with different weight percentages of MgH_2 powder. The microstructure and the elemental mapping of the composite fabricated using a 25 wt% MgH_2–(3Ti–B_4C) preform reveal a reasonably uniform distribution of reinforcing phases, as a network of TiC_x and TiB_2 without any residual intermediate phases as shown in Figure 3. The elemental mapping reveals the existence of Al (AZ91 contains 9 wt% Al) not only inside the Mg matrix but also in the Mg-free regions proving the formation of the ternary compound (Ti_2AlC).

The XRD results reveal that the volume percentage of Mg in the fabricated composites increased after adding MgH_2 powder to the 3Ti–B_4C preform as shown in Figure 4. However, more MgO was detected due to the decomposition of MgH_2 at low temperature forming Mg with high affinity to oxygen due, in part, to its high surface area. This high chemically reactive Mg in the preform reacted with B_4C and therefore, enhanced the reaction in the (Mg–Ti–B_4C) system and as a result, Mg composites were fabricated without any retained Ti, boron carbide, or any intermediate phases such as TiB or MgB_2.

XRD analysis revealed the formation of TiC_x and TiB_2 in all the composites that were fabricated with different amounts of MgH_2 in the preforms. The percentage of TiC_x decreases with increasing the weight percentage of MgH_2 in the preform. This is due to formation of Ti_2AlC at the expense of TiC_x. Ti_2AlC forms by the diffusion of Al from molten AZ91 alloy into the substoichiometric TiC_x at high temperature. The amount of Ti_2AlC is higher when using MgH_2 in the preform. The reason behind this is that the presence of MgH_2 in the preform accelerates the reaction and therefore, the formation of substoichiometric TiC_x is faster allowing more formation of this ternary compound compared with the case without MgH_2 in the preform for the same holding time.

1.2. Characterization of the TiC–TiB_2/Mg Matrix Composites

1.2.1. Density of the Composite

The bulk density of the TiC_x–TiB_2/AZ91D composites fabricated at 900 °C for 1.5 h using a 3Ti–B_4C preform and after

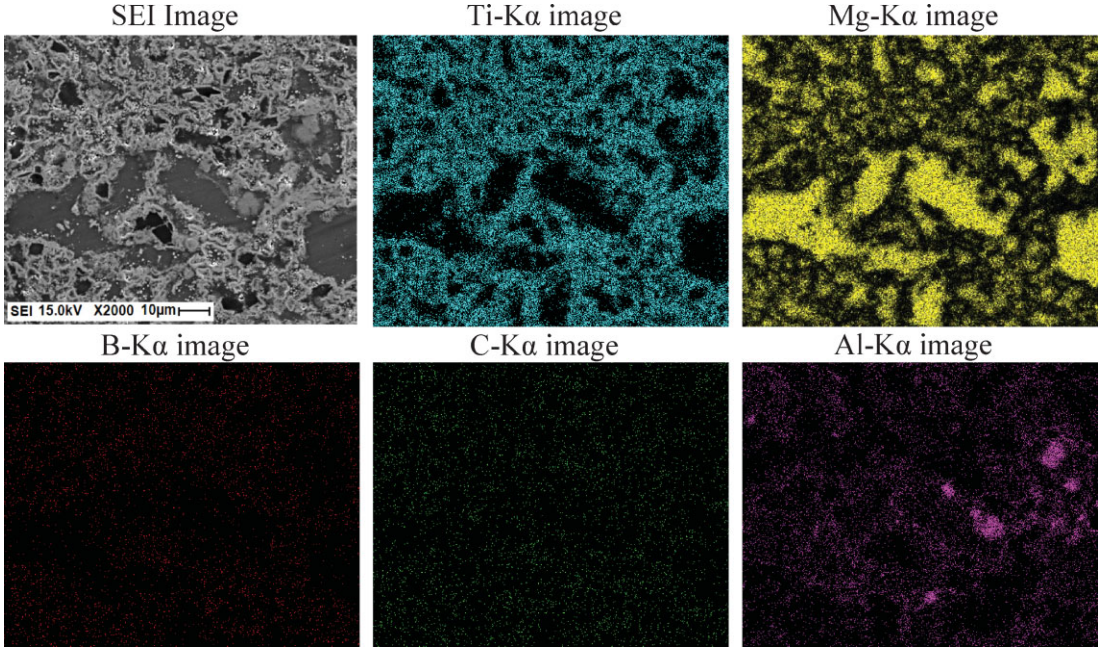

Fig. 3. SEM microstructure and EDS elemental mapping of the TiC_x–TiB_2/AZ91D composites synthesized at 900 °C for 1.5 h using a 25 wt% MgH_2–(3Ti–B_4C) preform with 70% RD.

DOI: 10.1002/adem.201200203

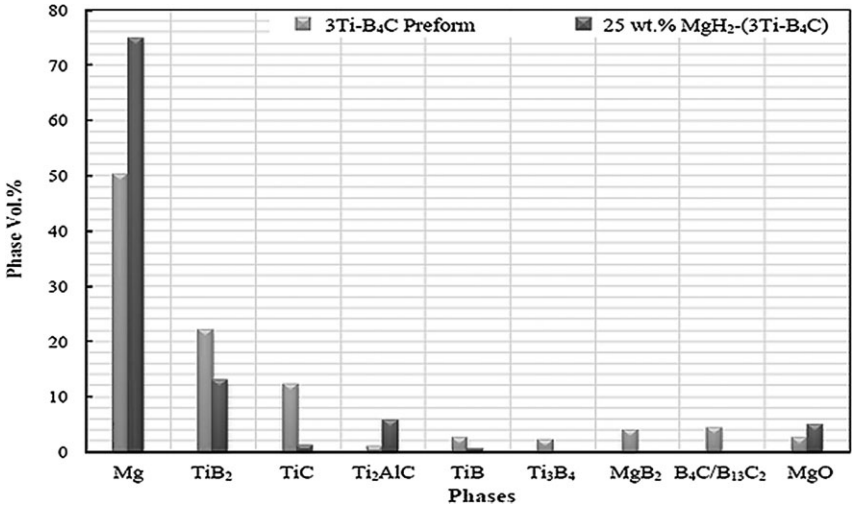

Fig. 4. Phase volume percentage of the MMCs fabricated at 900 °C for 1.5 h using two different 70% RD preforms: 3Ti–B_4C and 25 wt% MgH_2–(3Ti–B_4C).

adding different weight percentages of MgH_2 powder to the preform was measured. The results are shown in Figure 5 compared with the density of the unreinforced AZ91D Mg alloy[13] and that of TiC.[14]

The results reveal that the density of the infiltrated composites decreases with increasing MgH_2 powder content in the preform due to the increased Mg matrix content. Based on these results, the density of the composites can be tailored by controlling the weight percentages of the MgH_2 powder added to the 3Ti–B_4C preform. For example, the density of TiC_x–TiB_2/AZ91D composites decreased by nearly 13, 20, and 28% after adding 10, 25, and 40 wt% MgH_2 powder to the 3Ti–B_4C preform, respectively.

1.2.2. Compression Test Results

The compression behavior of the TiC_x–TiB_2/Mg composites fabricated at different processing parameters has been studied to obtain the parameters required to fabricate sound composites with improved mechanical properties. Furthermore, the compression behavior of the composites with different volume fractions of the reinforcing particles fabricated at these processing parameters has been investigated.

1.3. Processing Parametric Study

In this section, the effect of the processing parameters on compression test results is investigated.

1.3.1. Effect of Processing Temperature

Typical stress–strain curves obtained for the composite samples fabricated at different processing temperatures of 800, 850, and 900 °C are shown in Figure 6. These composites were fabricated using a 3Ti–B_4C preform with 70% RD at 1.5 h holding time.

It can be observed that the compressive strength and Young's modulus are affected significantly by the processing temperature. It is clear that the compressive strength and Young's modulus increased with increasing the processing temperature while the % height reduction decreased. There is a strong relation between the processing temperature and the mechanical properties obtained from the compression test.

According to the volume percentages of the phases from Retvield analysis, the highest volume fractions of the reinforcing phases, TiC_x and TiB_2, were found in the sample fabricated at 900 °C with very small retained boron carbide and residual intermediate phases compared with those fabricated at 800 or 850 °C. Therefore, the composites fabricated at 900 °C had the highest compressive strength and Young's modulus but the lowest ductility.

In general, the strength of the composite increased due to the formation of the reinforcing phases where the dispersion of fine and hard particles into the matrix blocks the dislocation motion and thus strengthens the material.

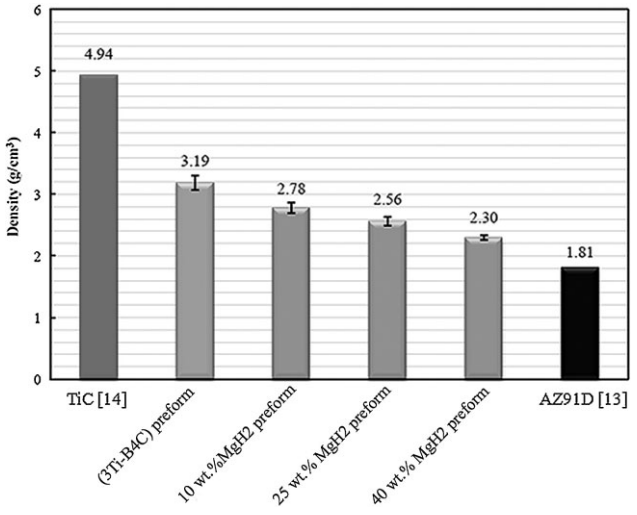

Fig. 5. Comparison of various bulk density values.

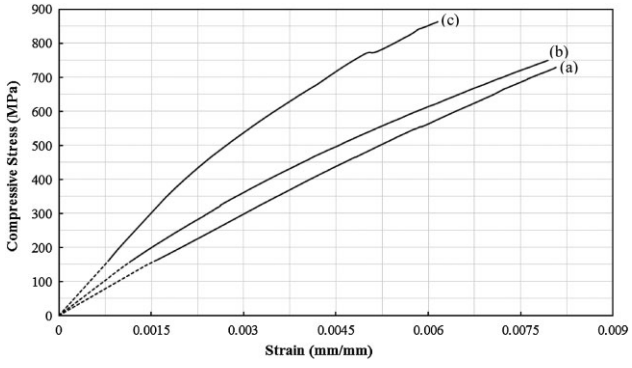

Fig. 6. Stress–strain curves of the TiC_x–TiB_2/AZ91D composites fabricated at different processing temperatures (a) 800 °C, (b) 850 °C, and (c) 900 °C.

ADVANCED ENGINEERING MATERIALS 2013,
DOI: 10.1002/adem.201200203

Table 1. Mechanical properties of the AZ91D alloy and TiC_x–TiB_2/AZ91D composites fabricated using 3Ti–B_4C preforms at different processing parameters.

Sample	Processing parameters			Young's modulus, E_{T160}, [GPa]	Compressive strength [MPa]	Height reduction [%]
	Temperature [°C]	Holding time [h]	Preform RD [%]			
AZ91D alloy	–	–	–	45	241	3.13
$(TiC–TiB_2)$/AZ91D composites	900 °C	1	70	144 ± 9.06	737 ± 25.26	0.72 ± 0.035
		1.5		195 ± 15.69	878 ± 19.47	0.66 ± 0.040
		3		161 ± 7.81	826 ± 26.80	0.76 ± 0.063
		1.5	60	115	639	0.80
			70	195 ± 15.69	878 ± 19.47	0.66 ± 0.040

1.3.2. Effect of Holding Time

The compression test has been performed on composites which are fabricated using 3Ti–B_4C preforms with 70% RD at 900 °C for different holding times: 1, 1.5, and 3 h. The average compressive strength, Young's modulus and the percentage of height reduction at different holding times are listed in Table 1.

It is clear that the holding time plays an important role in the fabrication of the composites and therefore, it can significantly affect their mechanical properties. The compression test results reveal that the composite sample fabricated at 1.5 h holding time has a higher compressive strength and Young's modulus than those of the samples fabricated at 1 or 3 h. For the composite fabricated at 900 °C for 1.5 or 3 h, the desired equilibrium phases, TiC_x, and TiB_2, formed with very small amounts of residual boron carbide and intermediate phases such as TiB and MgB_2. However, the formation of the ternary compound (Ti_2AlC) at 3 h adversely affects the compressive strength and the Young's modulus of the composite while at the same time can raise its ductility. On the other hand, the residual boron carbide and intermediate phases such as TiB and MgB_2 for composites fabricated at 1 h are higher than those at 1.5 or 3 h. For this reason, it has a lower compressive strength and Young's modulus than those of composites fabricated at 1.5 or 3 h.

Based on these results, it can be said that the composites fabricated at 900 °C for 1.5 h are stiffer and stronger than those fabricated at 900 °C for 1 or 3 h but they are more brittle.

1.3.3. Effect of Green Compact Relative Density

The influence of the preform RD on the compression behavior of the fabricated composites was investigated by testing different composite samples which have been fabricated at 900 °C for 1.5 h using 3Ti–B_4C preform with different relative densities. Table 1 lists the average compressive strength, Young's modulus and the percentage of height reduction.

The results reveal the great effect of the preform RD on the compressive strength and Young's modulus of the fabricated TiC_x–TiB_2/AZ91D composites. The green compact RD plays an important role in the fabrication of the composites and hence, it can significantly affect their mechanical properties. The compression test results reveal that using 70% green compact RD results in a higher compressive strength and Young's modulus than those fabricated using 60%. This is because the larger the green compact RD, the higher the contact area between B_4C and Ti particles thus accelerating the reaction between them through a shorter diffusion path and hence affecting the microstructure and the formed phases in the composite.

In summary, considering that the compressive strength and Young's modulus of the unreinforced AZ91D matrix are ≈240 MPa and 45 GPa, respectively, the compressive strength and Young's modulus of the composites fabricated using a 3Ti–B_4C preform with 70% RD at 900 °C for 1.5 h increased by nearly 265 and 333%, respectively. However, the composites are brittle due to the high volume fractions of the reinforcing phases of the hard ceramic particles.

1.4. Compression Behavior of Composites Fabricated using MgH_2–(3Ti–B_3C) Preform

In an attempt to improve the ductility of the fabricated composites by increasing the volume percentage of the Mg matrix, composite samples using MgH_2–(3Ti–B_4C) preforms with 70% RD were fabricated at 900 °C for 1.5 h. Different weight percentages of MgH_2 powder in the preform have been used while the molar ratio of Ti:B_4C was kept at 3:1.

1.4.1. Tailoring the Mechanical Properties of the TiC_x–TiB_2/AZ91D Composites

Typical compression behavior of the TiC_x–TiB_2/AZ91D composites reinforced with different volume percentages of the reinforcing phases due to the use of MgH_2 powder in the 3Ti–B_4C preform compared with that of the unreinforced AZ91D alloy is given in Figure 7. The compression test results for these composites are summarized in Table 2.

It is clear that the strength and stiffness of the composites increase in response to the higher content of the reinforcing phases, TiC_x and TiB_2. The compression test results show that the composites fabricated using a 3Ti–B_4C preform are stiffer and stronger than those fabricated after adding MgH_2 powder to the preform. On the other hand, the ductility of the composites was improved substantially by nearly 26, 81, and 187% by adding 10, 25, and 40 wt% MgH_2 powder to the 3Ti–B_4C preform, respectively. This is due to the increase of the Mg matrix volume fraction in the fabricated composites.

DOI: 10.1002/adem.201200203

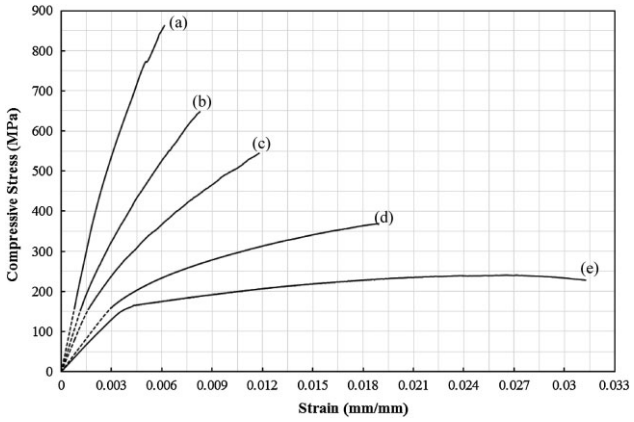

Fig. 7. Stress–strain curves of the composites fabricated using MgH_2–(3Ti–B_4C) preform with different MgH_2 contents: (a) 0 wt%, (b) 10 wt%, (c) 25 wt%, (d) 40 wt%, and (e) the AZ91D alloy.

The average compressive strength and Young's modulus of the fabricated composites decreased from ≈878 MPa and 195 GPa, with 0 wt% MgH_2 in the preform to ≈370 MPa and 55 GPa when 40 wt% MgH_2 powder is added to the preform. This means that the strength and stiffness decreased by about 58 and 72% after adding 40 wt% MgH_2 while the ductility was improved by about 187%.

It can be concluded that although the compressive strength and stiffness of the fabricated composites decreased significantly by adding MgH_2 powder to the preform, their ductility was significantly improved. Hence, the mechanical properties of the composites can be tailored by controlling the amount of MgH_2 addition in the MgH_2–(3Ti–B_4C) preform.

1.5. Flexural Strength Test Results

1.5.1. Flexural Strength Results of the TiC_x–TiB_2/AZ91D Matrix Composites

The experimental flexural strength results for the composites fabricated using a 3Ti–B_4C preform and after adding different weight percentages of MgH_2 powder to the preform are presented in Figure 8.

The results show that the average flexural strength of the TiC_x–TiB_2/AZ91D composites fabricated using a 3Ti–B_4C preform is ≈419 MPa which is higher than the ultimate strength of the AZ91D alloy (250 MPa[13]) by ≈68% while it is lower than the flexural strength of TiC (560 MPa[14]) by ≈25%. Also, the results reveal the effect of the volume fraction of the reinforcing network controlled by varying the weight percentage of MgH_2 powder. The results show that the flexural strength of the composites decreased with decreasing the volume fractions of the reinforcing phases, TiC_x and TiB_2, through adding different weight percentages of MgH_2 powder to the 3Ti–B_4C preform.

Looking at the individual results (Figure 8), the average flexural strength of the composites decreased by 19, 26, or 44% due to adding 10, 25, or 40 wt% MgH_2 powder. These results show that the composites, fabricated using just a 3Ti–B_4C preform have higher strength but are more brittle. However, ductility increased with increasing the volume fraction of Mg matrix in the composites by adding MgH_2 powder to the preform.

1.6. Fractographic Analysis

Knowledge about the behavior of Mg matrix composites under different loading conditions is required especially as these composites are used in different applications. Therefore, the investigation of failure mechanisms of Mg alloys and their composites is essential.[15]

In this study, the fractured surfaces of the composite samples were analyzed after the four-point bending test. SEM with EDS spot analysis was employed to determine the failure mechanisms of the TiC_x–TiB_2/Mg composite. Figure 9 shows the general fracture surface area of the composites fabricated using a 3Ti–B_4C preform with 70% RD at the 900 °C for 1.5 h.

Fracture surfaces were flat and parallel to the applied load when viewed at a macroscopic scale but rough when viewed by a microscope as shown in Figure 9a. The flat appearance of the fractured surfaces indicating brittle behavior is because of the high TiC_x–TiB_2 content.

At higher magnification as shown in Figure 9b, signs of mixed fracture are shown in the AZ91D matrix. SEM observations show cleavage regions as flat areas, which are related to brittle failure while some microdimples also appear and are related to ductile failure. The dimples are small and shallow, consistent with the quite low ductility of the composite. This can be attributed to the HCP crystal structure of Mg that restricts the slip to the basal plane.[16]

For more details about the fracture mechanism, the SEM micrographs have been taken at different areas but at higher magnification combined with EDS spot analysis as shown in Figure 9c–e.

Table 2. Compression test results of the AZ91D alloy and TiC_x–TiB_2/AZ91D composites fabricated using MgH_2–(3Ti–B_4C) preform with different MgH_2 contents.

Sample	MgH_2 content in the preform	Reinforcing phases [vol%]	Young's modulus, E_{T160}, [GPa]	Compressive strength [MPa]	Height reduction [%]
AZ91D	–	–	45	241	3.13
TiC_x–TiB_2/AZ91D composites	0 wt%	≈40	195 ± 15.69	878 ± 19.47	0.66 ± 0.040
	10 wt%	≈30	134	648	0.83
	25 wt%	≈22	110 ± 10.01	540 ± 14.55	1.19 ± 0.068
	40 wt%	≈12	55	369	1.89

ADVANCED ENGINEERING MATERIALS 2013,
DOI: 10.1002/adem.201200203

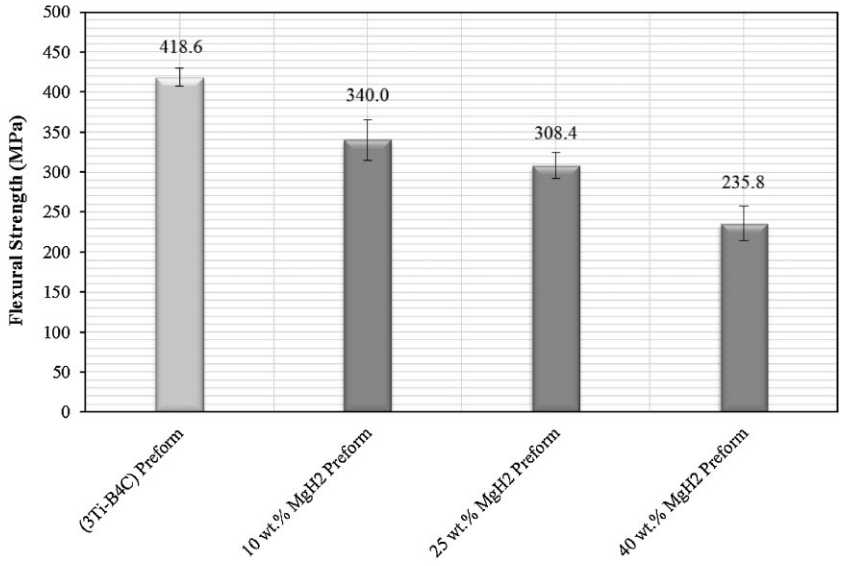

Fig. 8. Flexural strength of composites fabricated with different MgH_2 contents.

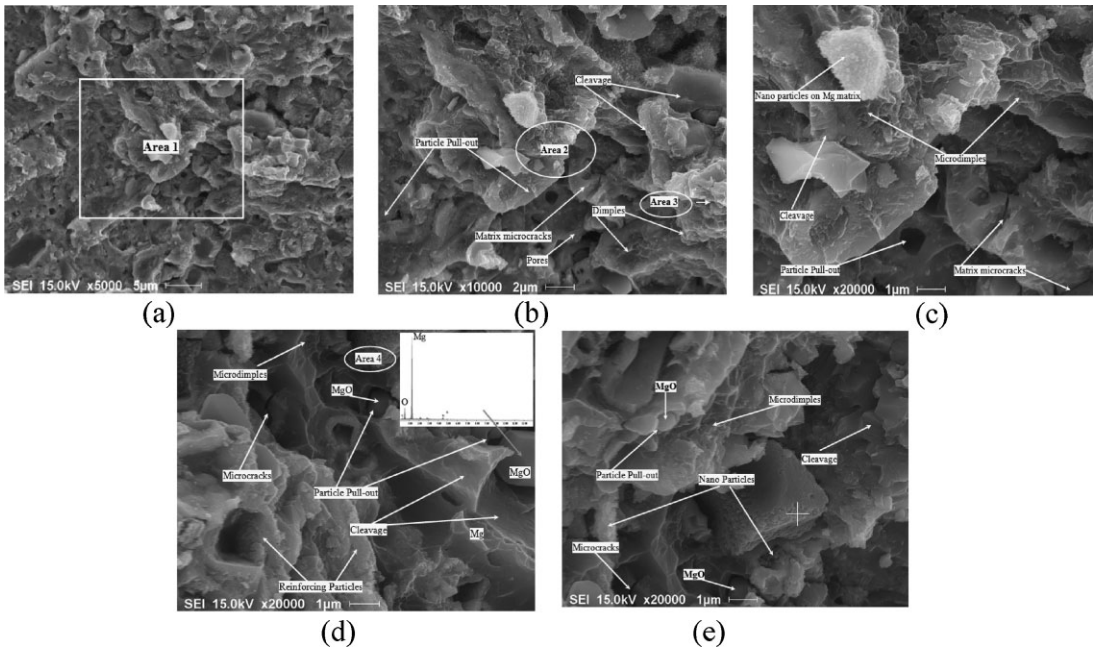

Fig. 9. SEM flexural fracture of $TiC_x–TiB_2$/AZ91D composite (a) at low magnification, (b) area 1 of (a), (c) and (d) areas 2, 3 of (b), and area 4 of (e) at high magnification.

Figure 9c (the magnified area 2 in Figure 9b) shows the fracture surface in more detail where the presence of few dimples in the Mg matrix can be observed in some regions while cleavage appears in other regions in the Mg matrix and in the ceramic particles. However, it is very difficult to notice the fracture in the particles or the presence of TiC/TiB_2 particles pull-out because the particles are very small and some of them are in the nano size. This indicates that the bonding between the matrix and the ceramic particle is very strong. Moreover, the SEM observations reveal some microcracks in the Mg and very small pores due to incomplete infiltration in between the particles or the shrinkage of the Mg matrix during cooling.

Furthermore, as shown in Figure 9d (magnified area 3 of Figure 9b), microdimples, and cleavage as well as the presence of microcracks in the Mg matrix are very clear. Also, MgO particle pull-out can be observed indicating that the bonding at the interface between the MgO particles and the Mg matrix is not strong. The existence of the dimples and cleavage in the Mg matrix was confirmed by the SEM/EDS spot analysis as shown in the figure. Also, the EDS spot analysis on the particles ''pulled-out'' proved that these particles are just

DOI: 10.1002/adem.201200203

MgO where Mg and oxygen are the only detected elements. For more details, Figure 9e (magnified area 4 of Figure 9d), reveals not only the presence of microdimples and cleavage besides the presence of microcracks in the Mg matrix but also MgO particles pull-out.

The fracture behavior of the composites fabricated using a preform containing MgH_2 powder is almost the same. However, the higher volume percentage of Mg reveals more microdimples but also more MgO particles pull-out.

Based on these observations, the composites exhibit a combination of completely brittle fracture regions and brittle-ductile fracture regions. In the brittle-ductile fracture regions, microdimples associated with Mg-enriched zones were observed in the matrix. In addition, microcracks observed in the matrix show that the failure might have initiated in the matrix rather than from the particulates.

2. Conclusions

1) Magnesium matrix composites with a relatively uniform distribution of the reinforcing TiC_x and TiB_2 phases were successfully fabricated using a practical and low cost in situ reactive infiltration technique.
2) The density of the composites can be tailored by controlling the weight percentages of the MgH_2 powder added to the $3Ti–B_4C$ preform.
3) The $TiC_x–TiB_2$/Mg matrix composites developed in this study exhibit higher modulus of elasticity and compressive strength compared with the unreinforced Mg matrix while the ductility is reduced.
4) The composites fabricated using $3Ti–B_4C$ preforms are stiffer and stronger than those fabricated after adding MgH_2 powder to the preform. For example, the strength and stiffness decreased by ≈58 and 72% after adding 40 wt% MgH_2 to the $3Ti–B_4C$ preform, while the ductility was improved substantially by nearly 187%.
5) The flexural strength of the composites is higher than the tensile strength of the unreinforced Mg alloy and decreased with increasing the weight percentage of MgH_2 powder in the preform.
6) The fracture surfaces after the flexural test revealed that the composites exhibit a combination of completely brittle fracture and brittle-ductile fracture regions.

3. Experimental Work

3.1. Fabrication of the Composites

In this work, titanium (−325 mesh, 99.61% purity, Alfa Aesar Co.) and boron carbide (99% purity, <10 μm particle size, Alfa Aesar Co.) powders at a molar ratio of 3:1 corresponding to that of stoichiometric TiC and TiB_2 were used to synthesize the ceramic reinforcing phases. The starting powders were mixed under Ar in a stainless steel jar with stainless steel balls inside a planetary ball mill. After full mechanical blending, the resulting mixture of Ti and B_4C powders was compacted at pressures ranging from 80 to 120 MPa into green compacts of cylindrical shape of 15 mm in diameter and variable heights with various relative densities of approximately 55, 60, 65, and 70 ± 2% using a hardened steel die with two plungers. The in situ reactive infiltration experiments were finally carried out in an electric furnace under the presence of flowing argon gas (purity ≥99.999%) as shown in Figure 10a. The temperature was set in the range from 700 °C to 950 °C at 50 °C intervals, the holding time ranged from 1 to 6 h and the heating rate was 10 °C min^{-1}. The samples were naturally cooled down to room temperature. MgH_2 powder (98% purity, <59 μm particle size, Alfa Aesar Co.) was added to the $3Ti–B_4C$ mixture at different weight percentages in an attempt to control the volume percentage of the reinforcing phases in the composites. The green compact $MgH_2–(3Ti–B_4C)$ was prepared in the same fashion as described above. MgH_2 powder was used in the preform instead of Mg powder because the decomposition of MgH_2 forms high chemically reactive Mg which accelerates the reaction in the $Mg–[MgH_2–(3Ti–B_4C)]$ system.

The bulk density of fabricated composites is measured using the water absorption method based on Archimedes principle (ASTM C20-00).[17] The microstructure and the phase analysis of the fabricated composite samples were investigated using SEM (Philips XL30 FEG) equipped with EDS and XRD using an (X'Pert PRO) X-ray diffractometer (PANalytical Inc.). It is important to note that Si is added to all powder samples during the XRD analysis as an internal standard to correct any systematic error.

3.2. Compression Test

The compression tests were conducted on as-received AZ91D alloy and $TiC–TiB_2$/Mg composites according to ASTM E9-89a [18]. Specimens were machined to a round cross-section of 12.7 mm (1/2 inch) in diameter and 25 mm (1 inch) in height. $TiC–TiB_2$/Mg matrix composites specimens were machined from the in situ reactive infiltrated material.

Testing was performed on MTS 809 equipment, with a 250 kN load capacity at room temperature with a cross-head speed of 0.5 mm min^{-1} (equivalent to a strain rate of 0.0003 s^{-1}) and no barreling was observed. To obtain strain measurements, two strain gauges (CEA-06-125UW-350, Vishay Micro-Measurements) were installed longitudinally parallel to the load direction on the side of each test sample with 180° between them as shown in Figure 10b.

The engineering stress was obtained by dividing the axial force by the initial cross-sectional area of each sample while the axial strain was evaluated using the two strain gauges placed in the longitudinal direction. Testing of three replicas of some selected samples have been performed to guarantee reliable results and to obtain the standard deviation.

Because the elastic portion of the stress–strain curve was not always linear, tangent elastic modulus was determined from the slope of the stress–strain curve at a fixed level of stress (160 MPa). This slope line is represented in the stress–strain curves by dotted lines.

ADVANCED ENGINEERING MATERIALS 2013,
DOI: 10.1002/adem.201200203

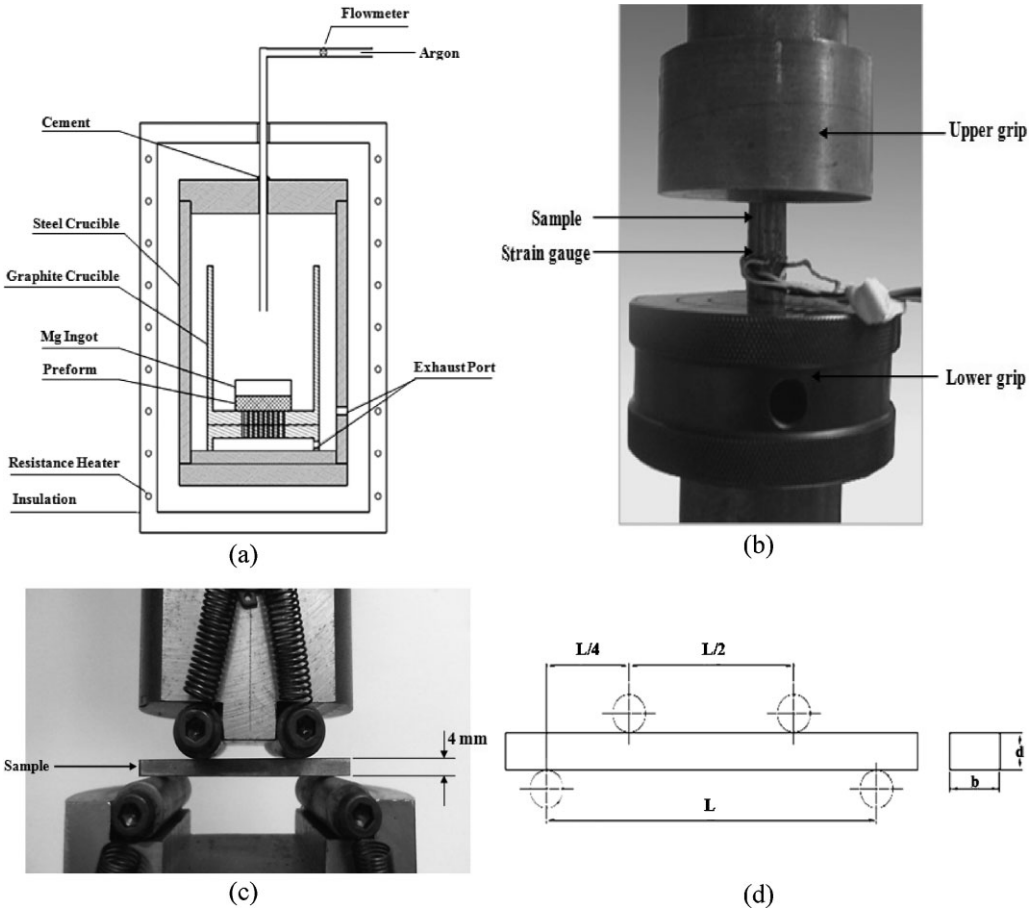

Fig. 10. (a) Schematic experimental set-up, (b) compression testing, (c) 4-point bending fixture, and (d) 4-point bending configuration.

Upon cooling of MMCs, residual stress is created due to the different coefficients of thermal expansion of the matrix and reinforcement causing dislocations to form at the ceramic/metal interface. In the present work, since the compression testing of the composite initially revealed non-linear elastic behavior, a cycling procedure was carried out to stabilize the dislocations in the matrix according to Prangnell et al. [19] By low load cycling, these dislocations were redistributed (or moved) from a high dislocation density region (matrix/reinforcement interface) to a lower one without damaging the composite material. For the low cycle compression test, the $TiC–TiB_2$/Mg composites were initially pre-strained to low level of stress, 25 MPa. On reaching 25 MPa, the stress was reduced to 5 MPa, followed by ten load cycles from 5 to 25 MPa at 0.1 Hz. After cycling, it was ramped down to 0 MPa. Young's modulus was determined from the slope of the linear stress–strain region.

This load cycling was also performed to ensure the integrity of the measurement procedure as in some cases; the strain gauges gave spurious outputs on initial load application to the compression samples. This was probably due to the lack of complete parallarity between sample and crosshead platens. The cycling action has allowed some ''bedding-in'' and produces consistent readings. In some cases, the stress–strain curve has been extrapolated back to zero loads using this cycled behavior to replace the erratic strain data on initial loading.

The Young's modulus obtained by the slope of the stress–strain curve at a fixed level of stress (160 MPa) was verified with the value of the slope of the stress–strain curve of the low cycle compression test done in the range from 5 to 25 MPa.

3.3. Flexural Test

Testing was done on a screw-driven Instron model 3382, with a load cell of 100 kN at a cross-head speed of 0.5 mm min^{-1}. In the present study, the flexural strength behavior of fabricated Mg matrix composites has been assessed at room temperature.

The four-point bending tests were conducted on the $TiC–TiB_2$/Mg composites according to ASTM 1161-02C [20]. The samples were ground using 240, 320, 400, 600, 800, and 1200 grit silicon carbide papers to achieve a mirror finish and to eliminate any residual stresses generated during cutting. The dimensions of the rectangular specimens are 4 mm × 6 mm × 50 mm. The samples were tested using a four-point bending fixture on an MTS machine where the load and support span are 20 and 40 mm, as shown in Figure 10c and d.

Received: May 24, 2012
Final Version: January 30, 2013

[1] E. Aghion, B. Bronfin, D. Eliezer, *J. Mater. Process. Technol.* **2001**, *117*, 381.
[2] B. L. Mordike, T. Ebert, *Mater. Sci. Eng. A* **2001**, *302*, 37.
[3] X. Zhang, H. Wang, L. Liao, X. Teng, N. Ma, *Mater. Lett.* **2005**, *59*, 2105.
[4] Y. Wang, H. Y. Wang, K. Xiu, H. Y. Wang, Q. C. Jiang, *Mater. Lett.* **2006**, *60*, 1533.
[5] H. Ye, X. Liu, *J. Mater. Sci.* **2004**, *39*, 6153.
[6] X. Zhang, L. Liao, N. Ma, H. Wang, *Mater. Res.* **2006**, *9*, 357.
[7] Q. F. Guan, H. Y. Wang, X. L. Li, Q. C. Jiang, *J. Mater. Sci.* **2004**, *39*, 5569.
[8] B. Ma, H. Y. Wang, Q. C. Jiang, *J. Mater. Sci.* **2005**, *40*, 4501.
[9] X. Zhang, H. Wang, L. Liao, X. Teng, N. Ma, *Mater. Lett.* **2005**, *59*, 2105.
[10] K. U. Kainer, in *Magnesium-Alloys and Technology*, Wiley-VCH Verlag GmbH & Co, Weinheim, Germany **2003**.
[11] W. Cao, C. Zhang, T. Fan, D. Zhang, *Mater. Trans.* **2008**, *49*, 2686.
[12] Y. Z. Lü, Q. D. Wang, W. J. Ding, X. Q. Zeng, Y. P. Zhu, *Mater. Lett.* **2000**, *44*, 265.
[13] M. M. Avedesian, H. Baker, in *Magnesium and Magnesium Alloys*, ASM International, Ohio, USA **1999**.
[14] J. F. Shackelford, W. Alexander, in *CRC Materials Science and Engineering Handbook*, Third edition, CRC Press, Boca Raton, FL **2001**.
[15] P. Palcek, A. Námešný, M. Chalupová, B. Hadzima, Failure Mechanisms in Magnesium Alloys Matrix Composites, *22nd DANUBIA-ADRIA Symposium on Experimental Methods in Solid Mechanics*, Parma, Italy, **2005**.
[16] X. Zhang, H. Wang, L. Liao, N. Ma, *J. ASTM Int.* **2005**, *3*(10), 1.
[17] ASTM standard C20-00, Standard test methods for apparent porosity, water absorption, apparent specific gravity, and bulk density of burned refractory brick and shapes by boiling water, West Conshohocken, PA, **2000**.
[18] ASTM E9-89a, Standard test methods of compression testing of metallic materials at room temperature, American Society for Testing and Materials, **1989**.
[19] P. B. Prangnell, T. Downes, W. M. Stobbs, P. J. Withers, *Acta Metall. Mater.* **1994**, *42*, 3425.
[20] ASTM C1161-02C, Standard test method for flexural strength of advanced ceramics at ambient temperature, American Society for Testing and Materials, Annual Book of Standards, West Conshohocken, PA, **2002**.

DOI: 10.1002/adem.201200203